Uncertainty in simulating twentieth century West African precipitation trends: the role of anthropogenic aerosol emissions

Paul-Arthur Monerie[1], Andrea J. Dittus[1], Laura J. Wilcox[1], and Andrew G. Turner[1,2]

[1]National Centre for Atmospheric Science, Reading, United Kingdom
[2]Department of Meteorology, University of Reading, Reading, United Kingdom

Paul-Arthur Monerie; https://orcid.org/0000-0002-5304-9559. p.monerie@reading.ac.uk

Andrea J. Dittus; https://orcid.org/0000-0001-9598-6869

Laura J. Wilcox; https://orcid.org/0000-0001-5691-1493

Andrew G. Turner; https://orcid.org/0000-0002-0642-6876

Key points

- Increases in anthropogenic aerosol emissions from North America and Europe can induce a decrease in West African precipitation

- The sensitivity to anthropogenic aerosol is an important factor in models' success in simulating the 1970s and 1980s drought over West Africa

- Uncertainty in anthropogenic aerosol forcing leads to uncertainties in trends in precipitation and temperature extremes over West Africa

Abstract

Anthropogenic aerosol emissions from North America and Europe have strong effects on the decadal variability of the West African monsoon. Anthropogenic aerosol effective radiative forcing is model dependent, but the impact of such uncertainty on the simulation of long-term West African monsoon variability is unknown. We use an ensemble of simulations with HadGEM3-GC3.1 that span the most recent estimates in simulated anthropogenic aerosol effective radiative forcing. We show that uncertainty in anthropogenic aerosol radiative forcing leads to significant uncertainty at simulating multi-decadal trends in West African precipitation. At the large scale, larger forcing leads to a larger decrease in the interhemispheric temperature gradients, in temperature over both the North Atlantic Ocean and northern Sahara. There are also differences in dynamic changes specific to the West African monsoon (locations of the Saharan heat low and African Easterly Jet, of the strength of the west African westerly jet, and of African Easterly Waves activity). We also assess effects on monsoon precipitation characteristics and temperature. We show that larger aerosol forcing results in a decrease of the number of rainy days and of heavy and extreme precipitation events and warm spells. However, simulated changes in onset and demise dates does not appear to be sensitive to the magnitude of aerosol forcing. Our results demonstrate the importance of reducing the uncertainty in anthropogenic aerosol forcing for understanding and predicting multi-decadal variability in the West African monsoon.

Plain language summary

The Sahelian drought of the 1970s and 1980s had consequences on agriculture, economy, and population migration, among others. The Sahelian drought is known to be partly caused by emissions of aerosol pollution from North America and Europe, leading to a reduction in rainfall for West Africa. However, the effect of aerosol pollution on atmospheric radiation – the light and heat that passes through the atmosphere – is uncertain, and the models we use to examine past and future climate change show a wide range of responses to these effects. We use a novel collection of simulations to assess the range of different outcomes for the West Africa monsoon based on this uncertainty in the effects of aerosol pollution. We show that simulations in which the atmosphere has a weak response to aerosol pollution do not reproduce the observed drying trend over West Africa, while simulations with a stronger atmospheric response to pollution feature a larger drought. This uncertainty in the effects of aerosol pollution leads to uncertain changes in the West African monsoon winds and rainfall and in extremes of rainfall and temperature.

1. Introduction.

The economies of West African countries strongly rely on the West African Monsoon (WAM) (Stige et al., 2006), which brings most of the total annual precipitation during the rainy season (Nicholson, 2013). The inter annual and multi decadal variability of the West African precipitation hence has strong societal impacts. For instance, a large drought hit the Sahel in the 1970s and 1980s (Lebel & Ali, 2009; Nicholson, 2013; Sanogo et al., 2015) and was associated with population migrations and economic loss. Since the 1990s, Sahel precipitation has increased (Lebel & Ali, 2009; Sanogo et al., 2015). This recovery coincides with a tripling of extreme storms (Taylor et al., 2012) and an increased flood risk (Elagib et al., 2021). Moreover, the economies of West African countries strongly rely on agriculture, which is strongly impacted by the timing of the monsoon (*i.e.,* onset and withdrawal dates) and by precipitation characteristics, such as the number of wet and dry spells. Therefore, predicting the multi-decadal evolution of Sahel precipitation is of paramount importance for populations across West Africa.

Pioneering studies have shown that there is a strong relationship between changes in sea surface temperature (SST) and precipitation across West Africa (Folland et al., 1984; Palmer, 1986; Rowell et al., 1992). SSTs in the Pacific, Indian, and Atlantic Oceans, and the Mediterranean Sea all influence West African climate, on a range of time scales (Fontaine et al., 2011). One of the main identified drivers of the Sahel drought is the shift to a negative phase of the Atlantic Multidecadal Variability (AMV) (Giannini et al., 2003; Mohino et al., 2011; Martin & Thorncroft, 2014; Monerie et al., 2019). Warming of Mediterranean SSTs is one of the main drivers of the Sahel precipitation recovery (Park et al., 2016). The Pacific Ocean also exercises control on decadal trends in precipitation, with a positive phase of the Interdecadal Pacific Oscillation leading to anomalously low Sahel precipitation in climate models (Villamayor & Mohino, 2015).

Simulated trends in West African monsoon precipitation have large biases, with models underestimating precipitation over West Africa (Monerie et al., 2020), as well as the decadal variability in Sahel precipitation (Biasutti, 2013). Nevertheless, models of the sixth phase of the Climate Model Intercomparison Project (CMIP6; (Eyring et al., 2016)) are generally successful in reproducing the sign of decadal trends of Sahel precipitation (Monerie et al., 2022). The ability of climate models to capture the sign of the decadal trends in Sahel precipitation, despite uncertainties in the magnitude, implies that these trends are influenced by external forcings, whose evolutions are shared by all climate models. Simulations have shown that the global increase in well-mixed Greenhouse gas (GHG) concentrations is associated with an increase in precipitation over the Sahel (Dong & Sutton, 2015; Herman et al., 2020; Marvel et al., 2020), while increasing European and North American anthropogenic aerosol emissions (AA) were a driver of the Sahel drought (Bonfils et al., 2020; Herman et al., 2020; Marvel et al., 2020; Hirasawa et al., 2020; Monerie et al., 2022). AA perturbs the heat budget, scattering shortwave radiation back to space, and changing cloud albedo and lifetime (Collins et al., 2017). Hence, the past increase in European and North American AA emissions was associated with a decrease in surface air temperature over the Northern Hemisphere, with a weakening of the interhemispheric temperature contrast (Friedman et al., 2013) and a southward shift of the West African monsoon circulation (Ackerley et al., 2011). Therefore, changes in AA emissions affect climate by changing SSTs (SST mediated) and land temperature (non-SST mediated). We still do not fully understand the main mechanism that allows AA to affect West African precipitation and we do not know how these mechanisms are sensitive to the magnitude of the AA forcing.

Since the 1980s, AA emissions have decreased over Europe and North America, contributing to a strengthening of the inter-hemispheric temperature contrast in favour of the Northern Hemisphere (Friedman et al., 2013) and a northward shift of the ITCZ and increase in Sahel

111 precipitation (Herman et al., 2020; Marvel et al., 2020; Hirasawa et al., 2020; Monerie et al.,
112 2022).
113

2. Open questions

We expect the effects of AA emissions on the West African precipitation to be uncertain (Shonk et al., 2020; Monerie et al., 2022). However, multi-model ensembles, where the effects of different aerosol forcings are difficult to untangle from the effects of other structural uncertainties, are typically used in attribution studies. Differences between climate models can for instance be due to either differences in AA radiative forcing (Myhre et al., 2014; Wilcox et al., 2015), to model formulation (Wilcox et al., 2015) and to mean state biases (Giannini et al., 2008; Biasutti, 2019; Monerie et al., 2020), which may in turn affect the ability of a model to simulate the response of the system to forcing. Thus, the role of uncertainty in AA radiative forcing on the simulation of the West African precipitation multi-decadal trend has not yet been quantified. The SMURPHS ensemble helps to overcome this issue by allowing an assessment of the effects of uncertainty in AA effective radiative forcing within a single model, isolating the role of forcing uncertainty. We use simulations that were designed to sample a plausible range of aerosol forcing, spanning most of the 95% confidence interval shown in IPCC AR5 (Boucher et al., 2013), for which the SMURPHS ensemble (Dittus et al., 2020) was designed. The SMURPHS ensemble was performed with HadGEM3-GC3.1, a CMIP6-generation climate model, with experiments forced by different levels of AA emissions (Figure 1). We then describe the simulation forced with the lowest AA emissions to be representative of a climate model that has a low AA forcing, and the simulation forced with the highest AA emissions to be representative of a model that has a high AA forcing.

Mechanisms that allow changes in AA emissions to affect the West African monsoon are still not well known. Studies focusing on the mechanisms mostly highlight large-scale changes in temperature (Ackerley et al., 2011). The direct atmospheric effect over land is the main driver of the changes in West Africa precipitation after an increase in AA emission in (Hirasawa et

al., 2020), while it is the changes in North Atlantic SSTs in (Zhang et al., 2022). Therefore, we can question the mechanisms allowing changes in AA emissions to affect West African precipitation. Here we assess effects of different forcing in AA on both large scale and regional scale drivers of the West African monsoon.

Beyond seasonal means, effects of AA emissions can lead to changes in precipitation characteristics. The focus of previous studies has been the mean change in West African precipitation (Giannini & Kaplan, 2019; Herman et al., 2020; Marvel et al., 2020), while effects on Sahel precipitation characteristics could have strong societal repercussions for the region's population, through changes in climate extremes and agricultural yield. AA emissions have a strong effect on temperature over the Sahara desert and West Africa (Ackerley et al., 2011) and could therefore also lead to changes in extreme precipitation events over the region, as shown for the recovery period (Taylor et al., 2017). Increases in AA emissions are associated with a drying over the tropics (Bonfils et al., 2020) and we can expect substantial impacts on the frequency of dry spell. AA emissions can also delay monsoon onset (Scannell et al., 2019; Song et al., 2021) and hence have further impacts on agriculture.

3. Data and methods

3.1 Data

3.1.1 Observations

We use observations to assess bias in precipitation and to compare simulated historical changes in precipitation to observed precipitation changes. We use several observations to ensure that results are not observation dependent. GPCP version-2.2 provides precipitation estimates over land and oceans, with 2.5° resolution in longitude and latitude, from January 1979 to present. GPCP incorporates precipitation estimates from satellite data and surface rain gauge observations (Adler et al., 2003). Precipitation data of the Global Precipitation Climatology Center (GPCC) version 7 (Schneider et al., 2014b) is available over global land from 1901 to Present, on a 0.5° x 0.5° horizontal resolution grid. We also use data from the Climate Research Unit (Harris et al., 2014) (CRU) version 4.03, which spans 1901-present and the data from the University of Delaware (UDEL; version 4.01) that is on a 0.5° horizontal resolution grid, available from 1901 to present (Willmott et al., 2001).

3.1.2 The SMURPHS ensemble

The simulations are performed with the coupled ocean-atmosphere general circulation model HadGEM3-GC3.1, hereafter referred to as HadGEM3. The atmosphere is at a N96 resolution (~135 km at mid-latitudes) and the ocean at the ORCA1 resolution (1° horizontal resolution) (Williams et al., 2018; Kuhlbrodt et al., 2018). HadGEM3 uses the GLOMAP two-moment aerosol scheme, which includes representation of aerosol effects on cloud albedo and lifetime (Mulcahy et al., 2020).

The simulations cover the historical CMIP6 period (1850-2014), and use the CMIP6 anthropogenic aerosol and precursor emission dataset (sulfur dioxide, black carbon, organic carbon) (Meinshausen et al., 2017; Hoesly et al., 2018). Five experiments are performed in

which historical AA emissions are scaled to sample a plausible range of historical aerosol forcing (Booth et al., 2018; Dittus et al., 2020), with five initial-condition members each. The resulting AA effective radiative forcing ranges from -0.38 Wm^{-2} to -1.50 Wm^{-2} and spans most of the 95% confidence interval presented in IPCC AR5 (Boucher et al., 2013). Five scaling factors were selected: x0.2 (-0.38 Wm^{-2}), x0.4 (-0.60 Wm^{-2}), x0.7 (-0.93 Wm^{-2}), x1.0 (-1.17 Wm^{-2}) and x1.5 (-1.50 Wm^{-2}) (Figure 1). The SMURPHS scalings hence spans the most recent estimates in simulated AA effective radiative forcing (Bellouin et al., 2020; Forster et al., 2021). The other forcing agents follow historical CMIP6 emissions and concentrations (Meinshausen et al., 2017; Dittus et al., 2020).

European and North American AA emissions have strong effects on West African precipitation (Marvel et al., 2020; Monerie et al., 2022). European and North American AA have increased from the end of the pre-industrial era to the 1980s and have decreased afterwards (Figure 1). The different scalings in the SMURPHS ensemble allow us to test the sensitivity of HadGEM3 to the magnitude of anthropogenic aerosol forcing, without additional uncertainties for structural differences between models.

3.1.3 CMIP6 single-forcing simulations

We use the aerosol-only (hist-aer) single forcing simulations of the Detection and Attribution MIP (DAMIP; (Gillett et al., 2016)) to assess effects of AA on a large set of CMIP6 models (Eyring et al., 2016). Historical aerosol-only simulations are forced by changes in AA forcing only other external forcings are kept constant (GHG, change in solar activity, volcanism). We use 3 ensemble members from each of 10 CMIP6 climate models (ACCESS-ESM1-5, BCC-

CSM2-MR, CanESM5, CNRM-CM6-1, FGOALS-G3, GISS-E2-1-G, HADGEM3-GC31-LL, IPSL-CM6A-LR, MIROC6, and MRI-ESM2-0) (See Table 2). For a comparison to the single-forcing experiments, the simulated historical change in West African precipitation is assessed using the DAMIP historical simulations.

3.2 Methods

We have used several metrics to quantify the effects of AA on drivers and characteristics of the monsoon and uncertainties therein.

3.2.1 West African precipitation

The West African precipitation index is computed as the weighted area average between 20°W and 20° and between 4°N and 12°N (See Figure 2a and Figure 3a). The West African precipitation index only account for land precipitation that fall from July to September.

3.2.2 Location of the Saharan Heat Low.

Meridional shifts in the location of the Saharan Heat Low (SHL) have substantial impacts on West African precipitation with a northward shift of the SHL associated with an increase in precipitation over West Africa (Lavaysse et al., 2009; Shekhar & Boos, 2017). We compute the low-level atmospheric thickness (LLAT; (Lavaysse et al., 2009)), defined as the difference between geopotential height at 700 hPa and 925 hPa. The location of the SHL is identified by selecting the latitude of the maximum of the LLAT zonal mean computed between 15°W and 30°E and from 0°N to 40°N, after cubic splines interpolation (Shekhar & Boos, 2017).

3.2.3 The West African Monsoon Index.

The West African Monsoon Index (WAMI) accounts for the strength of the monsoon circulation, quantifying vertical wind shear. The WAMI index (Fontaine et al., 1995) is computed as $WAMI = M925 - U200$ where *M925* is the standardized anomaly (divided by the standard deviation of the time series) of the wind modulus at 925 hPa and *U200* is the standardized anomaly of the zonal component of the wind at 200 hPa.

3.2.4 Location of the intertropical convergence zone and of the West African monsoon precipitation rain band.

The location of the intertropical convergence zone (ITCZ) is defined as the barycentre of the zonal mean of the precipitation, averaged across all longitudes and between 30°S and 30°N (Monerie et al., 2013; Shonk et al., 2020). The location of the West African monsoon precipitation rain band is defined in the same way as for the ITCZ but from precipitation between 10°W and 10°E and between 0° and 30°N (Monerie et al., 2013).

3.2.5 Cross-equatorial heat transport.

The meridional heat transport plays a fundamental role in governing the effects of external forcings on monsoon circulations (Biasutti et al., 2018). We compute the atmospheric heat transport (AHT) as the difference between the net heat budget at the top of the atmosphere and the net heat budget at the surface, following Trenberth & Caron (2001). We then compute the zonally integrated cumulative sum from south to north. The global average fluxes are subtracted from AHT (Magnusdottir & Saravannan, 1999) for each simulation. The cross-equatorial heat transport is defined as the average, over the equator, in AHT. We found negative values of cross-equatorial heat transport of ~2 PW in HadGEM3 in July-August-September, which are consistent with previous studies (Biasutti et al., 2018) (not shown).

Positive values of cross-equatorial heat transport denote a zonal mean transport from the southern to the northern hemisphere.

3.2.6 Moist static energy framework.

We describe changes in West African monsoon circulation using a moist static energy (MSE) framework. MSE allows quantification of the transformation of lower troposphere enthalpy and latent energy into geopotential energy in the upper levels, which is the main signal of convection. MSE is therefore directly related to monsoonal precipitation (Fontaine & Philippon, 2000; Bordoni & Schneider, 2008; Biasutti et al., 2018). MSE is defined as:

$$MSE = gz + C_pT + Lq$$

where gz is the geopotential energy, with g the gravitational acceleration and z the geopotential height. C_pT is the enthalpy, with C_p the specific heat of dry air at constant pressure, and T the temperature. Lq is the latent energy associated with evaporation and condensation of water, with L the latent heat of evaporation and q the specific humidity. MSE is integrated between the surface and 700 hPa.

The dry static energy is also defined, and does not account for changes in latent energy:

$$DSE = gz + C_pT$$

3.2.7 African Easterly Waves.

Over West Africa, precipitation variability is related to the synoptic activity of African Easterly Waves (AEWs) that are associated with mesoscale convective systems and sub-seasonal precipitation variability (Mekonnen et al., 2006). We use a proxy of the AEW activity, defined as the variance of the daily meridional wind at 850 hPa (Mekonnen et al., 2006; Skinner et al., 2012), filtering daily data with a 3-5 day band-pass filter (Diedhiou et al., 1999). We found that in HadGEM3 the 850 hPa meridional wind variance has a

maximum over the eastern tropical Atlantic and over West Africa, between 5°N and 25°N, and west of the Greenwich meridian as in reanalysis (Mekonnen et al., 2006).

3.2.8 Extreme indices.

We compute a set of extreme indices using the Expert Team on Climate Change Detection and Indices (ETCCDI) (Sillmann et al., 2013). First, we defined a wet day as a day on which precipitation exceeds 1 $mm.day^{-1}$. The simple daily intensity (SDII) is defined as the daily precipitation mean on wet days. R1mm is the number of wet days. R10mm and R20mm are the number of days for which precipitation amount exceeds 10 and 20 mm respectively. R10mm then documents heavy precipitation days and R20mm very heavy precipitation days. R95p documents the very wet days and is the daily mean precipitation of wet days that exceed the 95^{th} percentile of precipitation on wet days. r95ptot is the percentage of total precipitation that is contributed by precipitation extremes (by R95p events), a high value indicating that total precipitation is controlled by heavy events on only a few days.

Dry spells (CDD) are defined as periods of at least 5 consecutive dry days (precipitation below 1 $mm.day^{-1}$). Warm spells are defined when daily mean temperature is higher than the 90^{th} percentile in daily temperature, over at least 6 consecutive days. The warm spell index (WSDI) is the number of warm spells in a season.

Extreme indices are computed here over the 1950-1980 period, using daily values.

3.3 Statistical significance.

The statistical significance of the difference between two experiments is defined using a Monte Carlo approach. Synthetic ensembles are constructed through randomly resampling the 10 simulations (5 ensemble members for each of two scaling experiments) and performing the ensemble mean of each synthetic 5 ensemble members (i.e., providing a total of 252 synthetic ensemble means). The synthetic ensemble means are used to create a matrix

298 of anomalies (252 x 252 size) between two synthetic ensemble means, providing a large
299 ensemble of synthetic ensemble mean differences. Differences between two scaling
300 experiments are then judged significant at the 5% level when stronger than 97.5% of the
301 randomly obtained synthetic ensemble-mean differences (two-sided test).

302

303

4. Results.

4.1 Trends in JAS West African precipitation

We first assess the ability of HadGEM3 to simulate West African precipitation, in July-August-September (JAS), relative to GPCP. We note that HadGEM3 has a dry bias over West Africa, and a wet bias over the tropical Atlantic Ocean, showing that the West African monsoon is located too far south in HadGEM3 (Figure 2a). This is a common bias in climate models (Monerie et al., 2020). Anomalies in West African precipitation between HadGEM3 and GPCP are associated with a systematic cold bias over the Saharan desert and a warm bias over the tropical Atlantic Ocean in the model (Okumura & Xie, 2004; Richter & Xie, 2008; Monerie et al., 2016) (Figure S1). We have replicated the analysis with other observations and show the precipitation bias to be consistent (Figure S2).

The West African precipitation (4°-12°N – 20°W-20°E) decreases throughout the 20th century in both observations and simulations (Figure 2b). The simulated drying becomes more severe when the scaling is increased, showing that AA emissions have a substantial drying effect on West African precipitation. Decadal precipitation variability is high over West Africa and the influence of aerosol uncertainty might not emerge relative to internal climate variability. Therefore, we quantify effects of the scalings and of internal climate variability to verify robustness of the effects of AA emissions on West African precipitation. To do so we used two methods. (a) The effect of scalings, i.e., uncertainty in the forced response, is obtained by computing the standard deviation across the SMURPHS ensemble, using the 5-member ensemble-means to represent the forced response for each scaling (i.e., inter-scaling standard deviation). (b) Internal climate variability is defined as the differences between ensemble-members of the same scaling, which arise due to a perturbation of the

initial conditions. The intra-scaling standard deviation is computed for each scaling experiment and subsequently averaged to provide an estimate of the role of internal variability. The effect of scalings is likely to exceed internal climate variability after the first decade of the 1900s (Figure 2c), when differences of forcing between scalings increase (Figure 1). Therefore, we analyse trends in precipitation over the period 1900-1980 (Figure 2d).

The negative trend in West African precipitation from 1900-1980 monotonically increases when increasing scaling (Fig. 2d), evidencing a substantial effect of the AA forcing. We resampled data to test the statistical significance of the differences of the 1900-1980 trends between each scaling (see Sect. 3.3). We show robust differences between the lowest and the highest scalings, which are not due to internal climate variability. Similarly, we note that the x1.5 scaling is significantly different to all other scalings, but we do not find significant differences between the x1.0 and the x0.7 scalings, and between the x0.2 and x0.4 scalings (Table 1). The finding of substantial impact of AA emissions on the Sahel drought is consistent with the literature (Ackerley et al., 2011; Giannini & Kaplan, 2019; Marvel et al., 2020; Hirasawa et al., 2020). The drying trend of the x0.2 scaling does not emerge from internal variability (Figure 1d). All other scalings show robust drying trends, with the x1.5 scaling producing a drying trend that is around three times stronger than for the x0.2 scaling (Figue 2d). Therefore, the ability of a climate model to simulate the historical drought over the Sahel is likely to depend strongly on the magnitude of its AA forcing. This also confirms that the past increase in AA emissions from Europe and North America is a driver of the Sahel drought of the 1970s and 1980s (Herman et al., 2020; Hirasawa et al., 2020; Monerie et al., 2022).

We compare uncertainty across the SMURPHS ensemble to uncertainty across the CMIP6 DAMIP aerosol-only ensemble. The ensemble-mean trend in 1900-1980 West African precipitation is comparable between the two ensembles, both showing a negative trend of similar intensity over West Africa due to AA emissions (Figure 2d). HadGEM3 is not an outlier at simulating effects of AA emissions on West African precipitation. In addition, we show that the SMURPHS ensemble spread covers a large proportion of the historical CMIP6 ensemble spread (Figure 2d). Although we cannot rule out effects of internal variability on West African precipitation, we suggest that most of the CMIP6 ensemble spread is due to differences between climate models at simulating AA radiative forcing.

Results of the SMURPHS ensemble show that the simulation of the effects of AA on West African precipitation determines whether a multi-decadal drought occurs. Uncertainty in the effects of AA therefore has strong consequences, affecting our ability to simulate and predict multidecadal variability in West African precipitation. Here, we then build upon the published literature and show that understanding better ensemble spread in AA effective radiative forcing is necessary for advancing our ability to project the future of Sahelian droughts.

In addition, we note that, after the 1980s, the precipitation does not increase in GPCC and UDEL, while precipitation increases in CRU. All observations show a northward shift in precipitation and the discrepancy between observations is mostly due to difference in the pattern of the precipitation recovery among observations (Figure S3). For the recovery period, the lowest (<=x0.4) and medium-to-highest scalings (>=x0.7) show strong differences, but recovery trends do not strengthen monotonically with scalings (Figure S4), with no robust differences between the x0.7, x1.0 and x1.5 scalings. Therefore, we do not have a strong effect of the scalings here for the recovery, and we only focused our analyses on the drought period.

4.2 Mechanisms of AA effects on Sahel precipitation trends

We show effects of anthropogenic aerosol forcing uncertainty on West African precipitation by displaying differences in 1900-1980 trends between the highest and lowest scalings (*i.e.*, x1.5 – x0.2) (Figure 3a). Differences between scalings are strong, with significant differences in West African precipitation trends (Figure 3a). We note that trends in precipitation are almost equally due to trends in evaporation as to trends in moisture flux convergence (P-E), showing importance of local precipitation recycling (Figure S5). Larger aerosol forcing results in a stronger weakening of the moisture flux (Figure 3a), and of the westerlies (Figure S6). Besides, the anomalously strong northerlies advect relatively dry and cold air from the north, reducing precipitation (Figure 3a) and surface-air temperature (Figure 3b), and weakening the monsoon circulation, as in (Hill et al., 2017). The strengthening of the westerlies, north of 20°N, and the weakening of the westerlies, south of 20°N, is consistent with the decrease of pressure over North Africa (Figure 3b). The southward shift of the monsoon and the weakening of the westerlies are associated with the decreased surface-air temperature over northern Africa (Figure 3b), which is a key driver of the monsoon dynamics (Hall & Peyrillé, 2006; Chadwick et al., 2019). In addition, the increase in AA emission is associated with a decrease in surface air temperature over the North Atlantic Ocean (Figure 3b), contributing to the decrease in precipitation over West Africa, as in Monerie et al., (2022). Sea-level pressure increases over western North Africa and decreases over the Sahel (Figure 3b), highlighting a weakening of the regional meridional pressure gradient, that is consistent with a southward shift of the monsoon and of the SHL.

Cross-sections show a weakening of the low-level (1000—850 hPa) westerlies, and a strengthening and southward shift of the African Easterly Jet (AEJ) (Figure 3c), both associated with a decrease in Sahel precipitation in observations (Grist & Nicholson, 2001;

Nicholson, 2013). However, feedbacks exist between soil conditions, the ITCZ, the SHL and the AEJ (Schubert et al., 1991; Cook, 1999; Thorncroft & Blackburn, 1999) and a southward shift of the AEJ is closely linked to a decrease in Sahel precipitation, but the causality chain is not directly assessed here. Moreover, the relationship between jets and Sahel precipitation is not clearly simulated in climate models (Whittleston et al., 2017). For instance, HadGEM3 has a strong bias in 200 hPa zonal wind, not simulating a clear Tropical Easterly Jet, which is located between 0° and 10°N and at around 200 hPa in observations (Nicholson, 2013). However, our results show changes of the monsoon circulation that are physically consistent with a decrease in Sahel precipitation, that is, a southward shift of the AEJ and a weakening of the low-level westerlies. In addition to the zonal winds, we show anomalies in omega (the vertical velocity expressed in pressure coordinates) (Figure 3d). Climatological negative values of omega indicate ascent and deep convection at 500-300 hPa and between 0°-4°N. Negative values of omega also highlight the shallow circulation, which is located between the surface and 700 hPa, between 10°N and 20°N (Figure 3d). Increasing AA emissions led to a strengthening of the deep convection (Figure 3d) and to an increase in precipitation (Figure 3a) over the Gulf of Guinea (0-4°N). Omega decreases, between 8°N and 14°N at 400 hPa, showing an inhibited deep convection over the Sahel (Figure 3d), which is consistent with the decrease in precipitation at these latitudes (Figure 3a). In addition, omega increases over the northern edge of the shallow circulation and decreases over its southern edge, indicating a southward shift of the monsoon circulation over the northern Sahel.

We show that the increase in US and European AA emissions (Figure 1) affects the West African precipitation by shifting the atmospheric circulation southward. This is consistent with previous studies, which have shown that the effect of AA on West African precipitation is mostly dynamic (Hirasawa et al., 2020), more specifically through shifts of the atmospheric circulation (Monerie et al., 2022).

4.3 Global energetics control on local physics

Changes in regional monsoon precipitation are connected to global mean anomalies in cross-equatorial heat transport and to the location and extent of the Hadley Cell (Kang et al., 2008; Biasutti et al., 2018). In addition, regional mechanisms (*e.g.*, the African easterly jet, the Saharan heat low) (Hall & Peyrillé, 2006) are well known identified drivers of the West African Monsoon. Changes in AA emissions can therefore affect the West African monsoon precipitation through mechanisms of both regional and global scales. We have documented regional changes in Section 4.2 and assess here how they are connected to changes of global scales, and we highlight uncertainties (*e.g.*, the SMURPHS ensemble spread).

An increase in AA emissions is associated with a decrease in surface-air temperature over the northern Hemisphere and hence with a weakening of the interhemispheric temperature contrast (Figure 4a). The cooling of the northern Hemisphere is in turn associated with a weakening of the southward cross-equatorial atmospheric heat transport (Figure 4a). The weakening of the southward cross-equatorial heat flux is associated with a southward shift of the ITCZ (Figure 4b; Donohoe et al., (2013); McGee et al., (2014); Schneider et al., (2014a); Biasutti et al., (2018)). Here we show that uncertainty in the strength of the simulated radiative effects of AA has strong effects on the simulated trends in cross-equatorial heat transport and in the location of the ITCZ. This leads to strong uncertainties in trends in precipitation over the tropics, on a spatial scale wider than West Africa (Shonk et al., 2020).

Anomalies in the meridional location of the WAM portion of the ITCZ are linked to global-scale anomalies, including the location of the global zonal mean ITCZ (Figure 4c) and thus to the change in cross-equatorial atmospheric heat transport and in the interhemispheric temperature contrast. The location of the WAM is well correlated with the anomalies in precipitation over West Africa (Figure 4d). For scalings x0.7 and larger, the WAM shifts southward, and the West African monsoon precipitation decreases. There is therefore a clear

link between large-scale mechanisms and regional changes in precipitation, after an increase in AA emissions.

An increase in AA radiative forcing is associated with a southward shift of the SHL (Figure 4e). The West African precipitation anomalies are also associated with anomalies in the latitudinal location of the SHL (Lavaysse et al., 2009; Shekhar & Boos, 2017). We show here that uncertainty in AA radiative forcing also leads to strong differences in trends of the latitudinal location of the SHL (Figure 4e), suggesting strong impacts of regional changes of the atmospheric circulation. In some cases, a northward shift of the SHL is associated with a decrease in West African precipitation (Figure 3e; scalings < 1.0), but we acknowledge that there is a strong ensemble-spread in the simulated trends in location of the SHL and anomaly in precipitation, for each scaling. Effects of internal variability stand out on regional scales. The shift in the location of the SHL is consistent with the changes in interhemispheric temperature gradient (Figure 4a) but shows a slightly different behaviour than global-scale changes because of the regional patterns in temperature anomalies. The southward shift of the SHL is also in line with a decrease in surface-air temperature over northern Africa, and with a southward shift of the monsoon (Figure 3b and Figure 4e).

The WAM circulation weakens with increasing emissions in AA (Figure 4f), through a decrease in zonal vertical wind shear (Fontaine et al., 1995). The low-level west African westerly jet weakens as well, explaining a part of the decrease in moisture flux convergence and precipitation over West Africa (Figure 4g) (Grodsky et al., 2003; Pu & Cook, 2010). The dynamics of the WAM is controlled by the meridional gradients in moist static energy, through changes in latent, sensible and geopotential energy between the hot Saharan desert and the humid Guinean zone (Fontaine & Philippon, 2000; Gaetani et al., 2017). We show meridional gradients in MSE in Fig. 4h (difference between 20°N-30°N and 5°N-15°N, averaged over longitudes 10°W-10°E). The climatological MSE gradient is negative because

the shape of the meridional gradient in MSE is mostly given by latent heat that is maximum over the Sahel (not shown). AA emissions affect the regional circulation by strengthening the meridional gradients in MSE (Figure 4h), suggesting a weakening of the WAM dynamics. We not that, unlike MSE, gradients in dry static energy (DSE) decreases when increasing scalings, also showing an effect of the decrease in Sahara temperature on monsoon circulation.

To summarise, the response to anthropogenic aerosol emissions is strongly dependent on the magnitude of the global forcing. Strong differences between scalings are noted in the responses of changes in meridional gradients in heat and energy, on the location of the monsoon circulation and on three-dimensional structure of the monsoon (*e.g.*, strength and location of the AEJ and SHL, vertical wind shear and vertical ascent). Therefore, uncertainties associated with the simulation of the effects of AA emissions are shown for the drivers of the West African monsoon on both large and regional scales. We show differences between large-scale and regional-scale mechanisms. For instance, the interhemispheric temperature gradient weakens in the x0.4 scaling relative to the x0.2 scaling, while differences in the location of the SHL are indistinguishable between the two scalings. Hence, we suggest that the large-scale view alone provides a first order explanation of the effects of AA on the West African precipitation but does not explain the full ensemble-spread in the West African precipitation trend. We acknowledge that all drivers are interconnected. The AEJ is for instance a consequence of both the surface dry gradient caused by the SHL, and the aloft heating caused by the precipitation in the WAM, and with the changes in soil conditions. Consequently, we note strong uncertainty in the drivers of the monsoon, due to a change in AA emissions, but cannot here define which of these mechanisms is dominant on the West African monsoon.

4.4 Precipitation characteristics and synoptic variability

We have documented the change in JAS precipitation over West Africa so far. However, a change in the monsoon goes beyond a change in the seasonal mean precipitation and may also include changes in monsoon onset date and season length, and changes to climate hazards such as the number of rainy days and storms or precipitation intensity. These aforementioned descriptors have strong societal effects on African countries, impacting agriculture yield (Sultan & Gaetani, 2016) and leading to drought or flood, among others.

African easterly waves (AEWs) favour deep convection and are associated with well organised mesoscale systems (Diedhiou et al., 1999; Mekonnen et al., 2006; Vellinga et al., 2016; Núñez Ocasio et al., 2020a) that cause precipitation extreme events (Crétat et al., 2015; Vellinga et al., 2016). The AEJ serves as a wave guide for the AEWs (Diedhiou et al., 1999) and the hydrodynamic instability of the AEJ can initiate and maintain AEWs (Carlson, 1969; Burpee, 1974; Núñez Ocasio et al., 2020b). Changes in the strength and location of the AEJ have effects on the AEWs, and thus on mesoscale and extreme precipitation. We show that increasing the strength of aerosol forcing is associated with a strengthening and a southward shift of the AEJ (Figure3b) and we therefore expect AEWs to be significantly impacted by AA. The southward shift of the AEJ is accompanied by a weakening of the barotropic instability over land (Figure S7), indicating a reduction of the conditions that can favour AEWs over West Africa (Wu et al., 2012). Consequently, we note a weakening of AEW activity (Figure S8), suggesting a weakening in the frequency of well-organised mesoscale systems, and a decrease in precipitation extreme events.

The precipitation intensity (SDII) is not dramatically reduced over most of the Sahel (Figure 5a) in response to aerosol increases. SDII decreases substantially over the tropical Atlantic Ocean, the western coast of West Africa, over Guinea and Sierra Leone, Liberia, and western

Senegal (Figure 5a). The number of rainy days (r1mm) decreases over West Africa and increases over the Gulf of Guinea (Figure 5b), accompanying a southward shift of the monsoon (Figure 3a; Figure 4b; Figure 4c).

The comparison of the patterns of anomalies in precipitation (Figure 3a), SDII (Figure 5a), and R1mm (Figure 5b) shows that uncertainty in precipitation anomaly, due to the increase in AA emission, is primarily due to uncertainty in the number of rainy days rather than to the intensity of rainy events. The decrease in the number of rainy days is associated with a decrease in the number of intense rainy days (R10mm; Figure 5c) and heavy rainy days (R20mm; not shown). We could therefore expect a change in precipitation to be associated with a change in the contribution of extreme precipitation to total precipitation amount, following Taylor et al., (2017). In HadGEM3 the percentage of precipitation that is due to extreme events is not dramatically affected by changes in AA radiative forcing (Figure 5d). However, the contribution of extreme precipitation events to total precipitation decreases over the western coast, consistently with a decrease in precipitation intensity (Figure 5a).

Differences in the AA radiative forcing leads to differences in the simulated number of dry spells over the Sahel, with higher AA scalings yielding to a higher number of dry spells during the rainy season (Figure 5e). This might lead to strong uncertainty when simulating effect of external forcing on crops and agricultural yield, as well as on human health. Wet spells are also affected by the change in AA radiative forcing, with a reduction in wet spells when increasing the scaling (Figure S9). Stronger scalings are associated with stronger decreases in temperature, hence potentially impacting temperature hazards. Heat waves have strong effect on human health, and we show that an uncertain AA radiative forcing would lead to difficulties in simulating, and thus at potentially predicting, these events (Figure 5f). We also show that an increase in European and North American AA emissions is associated with a decrease in the warm spell frequency.

We computed onset and withdrawal dates of the monsoon over West Africa, using an anomaly cumulative function with daily precipitation (Liebmann et al., 2012). We find significant differences between scalings on the onset date of the monsoon, over Niger (Figure S10 and method in supplementary material). However, the differences between scalings are not significant over most of the West African region, and we do not find differences between scalings when averaging the changes in onset date over West Africa (4°-12°N – 20°W-20°E) (Figure S11). The uncertainty in AA radiative forcing does not affect the simulated change in the demise date in HadGEM3 (not shown). This result contrasts with previous findings (Song et al., 2021) which attributes historical delay of West African precipitation to changes in greenhouse gases and AA emissions.

5. Conclusions and discussion

The SMURPHS ensemble consists of simulations with scaled emissions of anthropogenic aerosol and precursors that reproduce the 90% confidence interval of best estimates of aerosol effective radiative forcing (Boucher et al., 2013; Bellouin et al., 2020; Dittus et al., 2020). We have used the SMURPHS ensemble to quantify the effects of uncertainty in anthropogenic aerosol radiative forcing on West African precipitation variability, with one climate model, so that the effects of forcing uncertainty are seen in isolation from model structural differences such as monsoon biases. We show that the SMURPHS ensemble is a good proxy of the CMIP6 ensemble, covering a large proportion of the range in CMIP6 West African historical precipitation trends associated with AA emissions (i.e., the single-forcing experiment of DAMIP (Gillett et al., 2016)).

We show the strong effect of uncertainty in AA radiative forcing on multi-decadal West African precipitation trends and characteristics, and on the West African monsoon dynamics. A low-AA radiative forcing (scaling x0.2) is associated with a negative 1900-1980 trend in West African precipitation that does not clearly emerge from internal variability, while a high-AA radiative forcing (scaling x1.5) is associated with a substantial drying over West Africa. Therefore, we show that the simulation of the historical drying over West Africa is strongly dependent on simulated AA radiative forcing. Climate models that have a low AA radiative forcing might not be suitable for predicting future long-lasting droughts over the Sahel, due to local and global changes in anthropogenic aerosol emissions. Climate models that have an anomalously high AA radiative forcing might also overestimate future droughts, leading to false alarms in predicting decadal changes in precipitation. In addition to better understanding uncertainty associated with internal variability (*e.g.*, the effects of Atlantic multidecadal variability) on West African precipitation, we then show that a better

588 understanding of the simulated effects of AA emissions on the West African monsoon is of
589 paramount importance for predictions and projections.

590 We show that uncertainty in AA radiative forcing leads to uncertainty in the simulation of
591 changes in precipitation characteristics, with larger forcing leading to stronger decreases in
592 the number of rainy days and heavy rain days. There is also a substantial uncertainty in
593 simulations of the number of dry and warm spells because of uncertainty in AA radiative
594 forcing. However, we show that the effect is not substantial when considering the
595 contribution to total precipitation from precipitation extreme events, or the onset and demise
596 dates of the West African monsoon, in HadGEM3. Uncertainties in the effects of AA in
597 climate models are a significant limitation for detection-and-attribution studies in changes in
598 extreme events and on impacts on public health, economy and on the agricultural sector.

599 We provide a first attempt at quantifying the impact of uncertainty in the strength of global
600 aerosol forcing on drivers of the West African monsoon, at both global and regional scales.
601 AAs scatter shortwave radiation back to space, reducing surface-air temperature. Therefore,
602 uncertainty in the effects of AA results in strong differences in trends of global mean surface
603 air temperature (Dittus et al., 2020) and of the interhemispheric temperature gradient. These
604 sources of uncertainty affect the simulations of the cross-equatorial heat transport and of the
605 shifts of the intertropical convergence zone. On a regional scale, we show that the response of
606 the West African monsoon system (westerlies, African easterly jet, location of the Saharan
607 heat low, and African easterly waves) has a strong, linear dependence on simulated AA
608 forcing. We also acknowledge that local changes in emissions in SO_2 also impact the West
609 African monsoon, but that differences in AA emission are small between scalings over West
610 Africa (not shown).

611

Effects of anthropogenic aerosols on climate exceed the effects of greenhouse gases at a decadal timescales (Bartlett et al., 2018). Simulations of future changes in West African precipitation could therefore be very sensitive to uncertainty in simulating the effects of anthropogenic aerosols for near-term projections (*e.g.*, 2020-2040, when there are large uncertainties in local and remote aerosol emissions (Lund et al., 2019)). Uncertainty will arise due to differences between climate models in simulating effects of AA and to differences among emission scenarios. Therefore, a further study could consist of analysing effects of future changes in anthropogenic aerosol emissions trajectories on changes in West African precipitation, with the DAMIP simulations (Gillett et al., 2016), using the single-forcing simulations and emissions of SSP245 (O'Neill et al., 2016). This will help emphasize the role of AA emissions in future evolution of the West African monsoon, and large ensembles can be used to document the model uncertainty.

While this study focuses only on the effects of uncertainty in the magnitude of aerosol radiative forcing, further uncertainties in the West African monsoon response to aerosol emission changes are likely to be associated with structural differences between models. Differences in model physics can result in differences in particle transportation, for instance, which could lead to differences in the pattern of aerosol radiative forcing, and the mechanisms by which the forcing leads to precipitation changes. Uncertainties in the response to aerosol forcing may also be influenced by mean-state biases in models. For example, HadGEM3-GC3.1 has a dry bias over West Africa, with a monsoon located too far south relative to observations. The bias could lead to a misrepresentation of the sensitivity of the West African monsoon to changes in AA emissions, biasing low the sensitivity to AA emissions. A caveat of the study is thus that results could be model-dependent, and further work is required to understand whether such biases moderate or enhance the uncertainties that arise from differences in the magnitude of aerosol forcing.

637 Analysis of the SMURPHS ensemble demonstrates that uncertainty in the simulation of West
638 African precipitation trends due to simulations of the effects of anthropogenic aerosols is
639 strong. We show that uncertainties in aerosol radiative forcing could prevent us from
640 successfully predicting decadal trends in West African precipitation, such as the drought of
641 the 1970s-1980s. We suggest that a deeper understanding of effects of AA would yield to a
642 better near-term prediction of changes in Sahel precipitation.

643

644
645 **Acknowledgments**. P-A Monerie, L. J. Wilcox and A. G. Turner were supported by the
646 EMERGENCE project under the Natural Environment Research Council (NERC grant
647 NE/S004890/1). A. J. Dittus was supported by the SMURPHS project (NERC grant NE/N006054/1).
648 We acknowledge the World Climate Research Programme's Working Group on Coupled Modelling,
649 which is responsible for CMIP, and we thank the climate modeling groups for producing and making
650 available their model output. For CMIP the U.S. Department of Energy's Program for Climate Model
651 Diagnosis and Intercomparison provides coordinating support and led development of software
652 infrastructure in partnership with the Global Organization for Earth System Science Portals.

653

654 **Data availability statement**. CMIP6 GCM output is available from public repositories, including
655 https://esgf-index1.ceda.ac.uk/search/cmip6-ceda/. Output from the SMURPHS climate model
656 ensemble is archived at the Centre for Environmental Data Analysis
657 https://catalogue.ceda.ac.uk/uuid/5808b237bdb5485d9bc3595f39ce85e3. GPCC and GPCP
658 Precipitation data are provided by the NOAA/OAR/ESRL PSL, Boulder, Colorado, USA, from their
659 website at https://psl.noaa.gov/. CRU Precipitation is provided by the Climate Research Unit, from the
660 website at https://crudata.uea.ac.uk/cru/data/hrg/.

661
662

References

Ackerley, D., Booth, B. B. B., Knight, S. H. E., Highwood, E. J., Frame, D. J., Allen, M. R., & Rowell, D. P. (2011). Sensitivity of Twentieth-Century Sahel Rainfall to Sulfate Aerosol and CO2 Forcing. *Journal of Climate*, *24*(19), 4999–5014. https://doi.org/10.1175/JCLI-D-11-00019.1

Adler, R. F., Huffman, G. J., Chang, A., Ferraro, R., Xie, P.-P., Janowiak, J., et al. (2003). The Version-2 Global Precipitation Climatology Project (GPCP) Monthly Precipitation Analysis (1979–Present). *Journal of Hydrometeorology*, *4*(6), 1147–1167. https://doi.org/10.1175/1525-7541(2003)004<1147:TVGPCP>2.0.CO;2

Bartlett, R. E., Bollasina, M. A., Booth, B. B. B., Dunstone, N. J., Marenco, F., Messori, G., & Bernie, D. J. (2018). Do differences in future sulfate emission pathways matter for near-term climate? A case study for the Asian monsoon. *Climate Dynamics*, *50*(5), 1863–1880. https://doi.org/10.1007/s00382-017-3726-6

Bellouin, N., Quaas, J., Gryspeerdt, E., Kinne, S., Stier, P., Watson-Parris, D., et al. (2020). Bounding Global Aerosol Radiative Forcing of Climate Change. *Reviews of Geophysics*, *58*(1), e2019RG000660. https://doi.org/https://doi.org/10.1029/2019RG000660

Biasutti, M. (2013). Forced Sahel rainfall trends in the CMIP5 archive. *Journal of Geophysical Research: Atmospheres*, *118*(4), 1613–1623. https://doi.org/10.1002/jgrd.50206

Biasutti, M. (2019). Rainfall trends in the African Sahel: Characteristics, processes, and causes. *Wiley Interdisciplinary Reviews: Climate Change*, *10*(4), e591. https://doi.org/doi:10.1002/wcc.591

Biasutti, M., Voigt, A., Boos, W. R., Braconnot, P., Hargreaves, J. C., Harrison, S. P., et al. (2018). Global energetics and local physics as drivers of past, present and future monsoons. *Nature Geoscience*, *11*(6), 392–400. https://doi.org/10.1038/s41561-018-0137-1

Bonfils, C. J. W., Santer, B. D., Fyfe, J. C., Marvel, K., Phillips, T. J., & Zimmerman, S. R. H. (2020). Human influence on joint changes in temperature, rainfall and continental aridity. *Nature Climate Change*, *10*(8), 726–731. https://doi.org/10.1038/s41558-020-0821-1

Booth, B. B. B., Harris, G. R., Jones, A., Wilcox, L., Hawcroft, M., & Carslaw, K. S. (2018). Comments on "rethinking the lower bound on aerosol radiative forcing." *Journal of Climate*, *31*(22), 9407–9412.

Bordoni, S., & Schneider, T. (2008). Monsoons as eddy-mediated regime transitions of the tropical overturning circulation. *Nature Geoscience*, *1*(8), 515–519. https://doi.org/10.1038/ngeo248

Boucher, O., Randall, D., Artaxo, P., Bretherton, C., Feingold, G., Forster, P., et al. (2013). Climate change 2013: the physical science basis. Contribution of Working Group I to the Fifth Assessment Report of the Intergovernmental Panel on Climate Change. *K., Tignor, M., Allen, SK, Boschung, J., Nauels, A., Xia, Y., Bex, V., and Midgley, PM, Cambridge University Press, Cambridge, UK*.

Boucher, O., Servonnat, J., Albright, A. L., Aumont, O., Balkanski, Y., Bastrikov, V., et al. (2020). Presentation and Evaluation of the IPSL-CM6A-LR Climate Model. *Journal of Advances in Modeling Earth Systems*, *12*(7), e2019MS002010. https://doi.org/10.1029/2019MS002010

Burpee, R. W. (1974). Characteristics of North African Easterly Waves During the Summers of 1968 and 1969. *Journal of Atmospheric Sciences*, *31*(6), 1556–1570. https://doi.org/10.1175/1520-0469(1974)031<1556:CONAEW>2.0.CO;2

Carlson, T. N. (1969). SOME REMARKS ON AFRICAN DISTURBANCES AND THEIR PROGRESS OVER THE TROPICAL ATLANTIC. *Monthly Weather Review*, *97*(10), 716–726. https://doi.org/10.1175/1520-0493(1969)097<0716:SROADA>2.3.CO;2

Chadwick, R., Ackerley, D., Ogura, T., & Dommenget, D. (2019). Separating the Influences of Land Warming, the Direct CO2 Effect, the Plant Physiological Effect, and SST Warming on Regional Precipitation Changes. *Journal of Geophysical Research: Atmospheres*, *124*(2), 624–640. https://doi.org/doi:10.1029/2018JD029423

Collins, W. J., Lamarque, J.-F., Schulz, M., Boucher, O., Eyring, V., Hegglin, M. I., et al. (2017). AerChemMIP: quantifying the effects of chemistry and aerosols in CMIP6. *Geoscientific Model Development*, *10*(2), 585–607. https://doi.org/10.5194/gmd-10-585-2017

Cook, K. H. (1999). Generation of the African easterly jet and its role in determining West African precipitation. *Journal of Climate*, *12*(5), 1165–1184.

Crétat, J., Vizy, E. K., & Cook, K. H. (2015). The relationship between African easterly waves and daily rainfall over West Africa: observations and regional climate simulations. *Climate Dynamics*, *44*(1), 385–404. https://doi.org/10.1007/s00382-014-2120-x

Diedhiou, A., Janicot, S., Viltard, A., de Felice, P., & Laurent, H. (1999). Easterly wave regimes and associated convection over West Africa and tropical Atlantic: results from the NCEP/NCAR and ECMWF reanalyses. *Climate Dynamics*, *15*(11), 795–822. https://doi.org/10.1007/s003820050316

Dittus, A. J., Hawkins, E., Wilcox, L. J., Sutton, R., Smith, C. J., Andrews, M. B., & Forster, P. M. (2020). Sensitivity of historical climate simulations to uncertain aerosol forcing. *Geophysical Research Letters*, *n/a*(n/a), e2019GL085806. https://doi.org/10.1029/2019GL085806

Dong, B., & Sutton, R. (2015). Dominant role of greenhouse-gas forcing in the recovery of Sahel rainfall. *Nature Climate Change*, *5*(8), 757–760. https://doi.org/10.1038/nclimate2664

Donohoe, A., Marshall, J., Ferreira, D., & Mcgee, D. (2013). The Relationship between ITCZ Location and Cross-Equatorial Atmospheric Heat Transport: From the Seasonal Cycle to the Last Glacial Maximum. *Journal of Climate*, *26*(11), 3597–3618. https://doi.org/10.1175/JCLI-D-12-00467.1

Elagib, N. A., Zayed, I. S. Al, Saad, S. A. G., Mahmood, M. I., Basheer, M., & Fink, A. H. (2021). Debilitating floods in the Sahel are becoming frequent. *Journal of Hydrology*, *599*, 126362. https://doi.org/https://doi.org/10.1016/j.jhydrol.2021.126362

Eyring, V., Bony, S., Meehl, G. A., Senior, C. A., Stevens, B., Stouffer, R. J., & Taylor, K. E. (2016). Overview of the Coupled Model Intercomparison Project Phase 6 (CMIP6) experimental design and organization. *Geoscientific Model Development*, *9*(5), 1937–1958. https://doi.org/10.5194/gmd-9-1937-2016

Folland, C. K., Parker, D. E., & Kates, F. E. (1984). Worldwide marine temperature fluctuations 1856--1981. *Nature*, *310*(5979), 670–673. https://doi.org/10.1038/310670a0

Fontaine, B., & Philippon, N. (2000). Seasonal evolution of boundary layer heat content in the West African monsoon from the NCEP/NCAR reanalysis (1968–1998). *International Journal of Climatology*, *20*(14), 1777–1790. https://doi.org/https://doi.org/10.1002/1097-0088(20001130)20:14<1777::AID-JOC568>3.0.CO;2-S

Fontaine, B., Janicot, S., & Moron, V. (1995). Rainfall anomaly patterns and wind field signals over West Africa in August (1958–1989). *Journal of Climate*, *8*(6), 1503–1510.

Fontaine, B., Gaetani, M., Ullmann, A., & Roucou, P. (2011). Time evolution of observed July–September sea surface temperature-Sahel climate teleconnection with removed quasi-global effect (1900–2008). *Journal of Geophysical Research: Atmospheres*, *116*(D4), n/a--n/a. https://doi.org/10.1029/2010JD014843

Forster, P., Storelvmo, T., Armour, K., Collins, W., Dufresne, J.-L., Frame, D., et al. (2021). Chapter 7: The Earth's energy budget, climate feedbacks, and climate sensitivity.

https://doi.org/10.25455/wgtn.16869671.v1

Friedman, A. R., Hwang, Y.-T., Chiang, J. C. H., & Frierson, D. M. W. (2013). Interhemispheric Temperature Asymmetry over the Twentieth Century and in Future Projections. *Journal of Climate*, *26*(15), 5419–5433. https://doi.org/10.1175/JCLI-D-12-00525.1

Gaetani, M., Flamant, C., Bastin, S., Janicot, S., Lavaysse, C., Hourdin, F., et al. (2017). West African monsoon dynamics and precipitation: the competition between global SST warming and CO2 increase in CMIP5 idealized simulations. *Climate Dynamics*, *48*(3), 1353–1373. https://doi.org/10.1007/s00382-016-3146-z

Giannini, A., & Kaplan, A. (2019). The role of aerosols and greenhouse gases in Sahel drought and recovery. *Climatic Change*, *152*(3), 449–466. JOUR. https://doi.org/10.1007/s10584-018-2341-9

Giannini, A., Saravanan, R., & Chang, P. (2003). Oceanic Forcing of Sahel Rainfall on Interannual to Interdecadal Time Scales. *Science*, *302*(5647), 1027 LP – 1030. Retrieved from http://science.sciencemag.org/content/302/5647/1027.abstract

Giannini, A., Biasutti, M., Held, I. M., & Sobel, A. H. (2008). A global perspective on African climate. *Climatic Change*, *90*(4), 359–383. https://doi.org/10.1007/s10584-008-9396-y

Gillett, N. P., Shiogama, H., Funke, B., Hegerl, G., Knutti, R., Matthes, K., et al. (2016). The Detection and Attribution Model Intercomparison Project (DAMIP~v1.0) contribution to CMIP6. *Geoscientific Model Development*, *9*(10), 3685–3697. https://doi.org/10.5194/gmd-9-3685-2016

Grist, J. P., & Nicholson, S. E. (2001). A Study of the Dynamic Factors Influencing the Rainfall Variability in the West African Sahel. *Journal of Climate*, *14*(7), 1337–1359. https://doi.org/10.1175/1520-0442(2001)014<1337:ASOTDF>2.0.CO;2

Grodsky, S. A., Carton, J. A., & Nigam, S. (2003). Near surface westerly wind jet in the Atlantic ITCZ. *Geophysical Research Letters*, *30*(19). https://doi.org/https://doi.org/10.1029/2003GL017867

Hall, N. M. J., & Peyrillé, P. (2006). Dynamics of the West African monsoon. In *Journal de Physique IV (Proceedings)* (Vol. 139, pp. 81–99). EDP sciences.

Harris, I., Jones, P. D., Osborn, T. J., & Lister, D. H. (2014). Updated high-resolution grids of monthly climatic observations – the CRU TS3.10 Dataset. *International Journal of Climatology*, *34*(3), 623–642. https://doi.org/10.1002/joc.3711

Herman, R. J., Giannini, A., Biasutti, M., & Kushnir, Y. (2020). The effects of anthropogenic and volcanic aerosols and greenhouse gases on twentieth century Sahel precipitation. *Scientific Reports*, *10*(1), 12203. https://doi.org/10.1038/s41598-020-68356-w

Hill, S. A., Ming, Y., Held, I. M., & Zhao, M. (2017). A Moist Static Energy Budget–Based Analysis of the Sahel Rainfall Response to Uniform Oceanic Warming. *Journal of Climate*, *30*(15), 5637–5660. https://doi.org/10.1175/JCLI-D-16-0785.1

Hirasawa, H., Kushner, P. J., Sigmond, M., Fyfe, J., & Deser, C. (2020). Anthropogenic aerosols dominate forced multidecadal Sahel precipitation change through distinct atmospheric and oceanic drivers. *Journal of Climate*, 1–56. https://doi.org/10.1175/JCLI-D-19-0829.1

Hoesly, R. M., Smith, S. J., Feng, L., Klimont, Z., Janssens-Maenhout, G., Pitkanen, T., et al. (2018). Historical (1750--2014) anthropogenic emissions of reactive gases and aerosols from the Community Emissions Data System (CEDS). *Geoscientific Model Development*, *11*(1), 369–408. https://doi.org/10.5194/gmd-11-369-2018

Kang, S. M., Held, I. M., Frierson, D. M. W., & Zhao, M. (2008). The Response of the ITCZ to Extratropical Thermal Forcing: Idealized Slab-Ocean Experiments with a GCM. *Journal of*

Climate, *21*(14), 3521–3532. https://doi.org/10.1175/2007JCLI2146.1

Kelley, M., Schmidt, G. A., Nazarenko, L. S., Bauer, S. E., Ruedy, R., Russell, G. L., et al. (2020). GISS-E2.1: Configurations and Climatology. *Journal of Advances in Modeling Earth Systems*, *12*(8), e2019MS002025. https://doi.org/10.1029/2019MS002025

Kuhlbrodt, T., Jones, C. G., Sellar, A., Storkey, D., Blockley, E., Stringer, M., et al. (2018). The Low-Resolution Version of HadGEM3 GC3.1: Development and Evaluation for Global Climate. *Journal of Advances in Modeling Earth Systems*, *10*(11), 2865–2888. https://doi.org/10.1029/2018MS001370

Lavaysse, C., Flamant, C., Janicot, S., Parker, D. J., Lafore, J.-P., Sultan, B., & Pelon, J. (2009). Seasonal evolution of the West African heat low: a climatological perspective. *Climate Dynamics*, *33*(2), 313–330. https://doi.org/10.1007/s00382-009-0553-4

Lebel, T., & Ali, A. (2009). Recent trends in the Central and Western Sahel rainfall regime (1990–2007). *Journal of Hydrology*, *375*(1–2), 52–64. https://doi.org/10.1016/j.jhydrol.2008.11.030

Li, L., Yu, Y., Tang, Y., Lin, P., Xie, J., Song, M., et al. (2020). The Flexible Global Ocean-Atmosphere-Land System Model Grid-Point Version 3 (FGOALS-g3): Description and Evaluation. *Journal of Advances in Modeling Earth Systems*, *12*(9), e2019MS002012. https://doi.org/10.1029/2019MS002012

Liebmann, B., Bladé, I., Kiladis, G. N., Carvalho, L. M. V, B. Senay, G., Allured, D., et al. (2012). Seasonality of African Precipitation from 1996 to 2009. *Journal of Climate*, *25*(12), 4304–4322. https://doi.org/10.1175/JCLI-D-11-00157.1

Magnusdottir, G., & Saravannan, R. (1999). The response of atmospheric heat transport to zonally-averaged SST trends. *Tellus A: Dynamic Meteorology and Oceanography*, *51*(5), 815–832. JOUR.

Martin, E. R., & Thorncroft, C. D. (2014). The impact of the AMO on the West African monsoon annual cycle. *Quarterly Journal of the Royal Meteorological Society*, *140*(678), 31–46. https://doi.org/10.1002/qj.2107

Marvel, K., Biasutti, M., & Bonfils, C. (2020). Fingerprints of external forcing agents on Sahel rainfall: aerosols, greenhouse gases, and model-observation discrepancies. *Environmental Research Letters*, *15*(8), 084023. Retrieved from http://iopscience.iop.org/10.1088/1748-9326/ab858e

McGee, D., Donohoe, A., Marshall, J., & Ferreira, D. (2014). Changes in ITCZ location and cross-equatorial heat transport at the Last Glacial Maximum, Heinrich Stadial 1, and the mid-Holocene. *Earth and Planetary Science Letters*, *390*, 69–79. https://doi.org/https://doi.org/10.1016/j.epsl.2013.12.043

Meinshausen, M., Vogel, E., Nauels, A., Lorbacher, K., Meinshausen, N., Etheridge, D. M., et al. (2017). Historical greenhouse gas concentrations for climate modelling (CMIP6). *Geoscientific Model Development*, *10*(5), 2057–2116. https://doi.org/10.5194/gmd-10-2057-2017

Mekonnen, A., Thorncroft, C. D., & Aiyyer, A. R. (2006). Analysis of Convection and Its Association with African Easterly Waves. *Journal of Climate*, *19*(20), 5405–5421. https://doi.org/10.1175/JCLI3920.1

Mohino, E., Janicot, S., & Bader, J. (2011). Sahel rainfall and decadal to multi-decadal sea surface temperature variability. *Climate Dynamics*, *37*(3), 419–440. https://doi.org/10.1007/s00382-010-0867-2

Monerie, P.-A., Roucou, P., & Fontaine, B. (2013). Mid-century effects of climate change on African monsoon dynamics using the A1B emission scenario. *International Journal of Climatology*, *33*(4). https://doi.org/10.1002/joc.3476

Monerie, P.-A., Sanchez-Gomez, E., & Boé, J. (2016). On the range of future Sahel precipitation projections and the selection of a sub-sample of CMIP5 models for impact studies. *Climate Dynamics*. https://doi.org/10.1007/s00382-016-3236-y

Monerie, P.-A., Robson, J., Dong, B., Hodson, D. L. R., & Klingaman, N. P. (2019). Effect of the Atlantic Multidecadal Variability on the Global Monsoon. *Geophysical Research Letters*, *46*(3), 1765–1775. https://doi.org/doi:10.1029/2018GL080903

Monerie, P.-A., Wainwright, C. M., Sidibe, M., & Akinsanola, A. A. (2020). Model uncertainties in climate change impacts on Sahel precipitation in ensembles of CMIP5 and CMIP6 simulations. *Climate Dynamics*, *55*(5), 1385–1401. https://doi.org/10.1007/s00382-020-05332-0

Monerie, P.-A., Wilcox, L. J., & Turner, A. G. (2022). Effects of anthropogenic aerosol and greenhouse gas emissions on Northern Hemisphere monsoon precipitation: mechanisms and uncertainty. *Journal of Climate*, 1–66. https://doi.org/10.1175/JCLI-D-21-0412.1

Mulcahy, J. P., Johnson, C., Jones, C. G., Povey, A. C., Scott, C. E., Sellar, A., et al. (2020). Description and evaluation of aerosol in UKESM1 and HadGEM3-GC3.1 CMIP6 historical simulations. *Geoscientific Model Development*, *13*(12), 6383–6423. https://doi.org/10.5194/gmd-13-6383-2020

Myhre, G., Shindell, D., & Pongratz, J. (2014). Anthropogenic and Natural Radiative Forcing. In Intergovernmental Panel on Climate Change (Ed.), *Climate Change 2013 – The Physical Science Basis: Working Group I Contribution to the Fifth Assessment Report of the Intergovernmental Panel on Climate Change* (pp. 659–740). Cambridge: Cambridge University Press. https://doi.org/DOI: 10.1017/CBO9781107415324.018

Nicholson, S. E. (2013). The West African Sahel: A Review of Recent Studies on the Rainfall Regime and Its Interannual Variability. *ISRN Meteorology*, *2013*, 1–32. https://doi.org/10.1155/2013/453521

Núñez Ocasio, K. M., Evans, J. L., & Young, G. S. (2020a). A Wave-Relative Framework Analysis of AEW–MCS Interactions Leading to Tropical Cyclogenesis. *Monthly Weather Review*, *148*(11), 4657–4671. https://doi.org/10.1175/MWR-D-20-0152.1

Núñez Ocasio, K. M., Evans, J. L., & Young, G. S. (2020b). Tracking Mesoscale Convective Systems that are Potential Candidates for Tropical Cyclogenesis. *Monthly Weather Review*, *148*(2), 655–669. https://doi.org/10.1175/MWR-D-19-0070.1

O'Neill, B. C., Tebaldi, C., van Vuuren, D. P., Eyring, V., Friedlingstein, P., Hurtt, G., et al. (2016). The Scenario Model Intercomparison Project (ScenarioMIP) for CMIP6. *Geoscientific Model Development*, *9*(9), 3461–3482. https://doi.org/10.5194/gmd-9-3461-2016

Okumura, Y., & Xie, S.-P. (2004). Interaction of the Atlantic Equatorial Cold Tongue and the African Monsoon. *Journal of Climate*, *17*(18), 3589–3602. https://doi.org/10.1175/1520-0442(2004)017<3589:IOTAEC>2.0.CO;2

Palmer, T. N. (1986). Influence of the Atlantic, Pacific and Indian Oceans on Sahel rainfall. *Nature*, *322*, 251. Retrieved from http://dx.doi.org/10.1038/322251a0

Park, J., Bader, J., & Matei, D. (2016). Anthropogenic Mediterranean warming essential driver for present and future Sahel rainfall. *Nature Clim. Change*, *6*(10), 941–945. Retrieved from http://dx.doi.org/10.1038/nclimate3065

Pu, B., & Cook, K. H. (2010). Dynamics of the West African westerly jet. *Journal of Climate*, *23*(23), 6263–6276.

Richter, I., & Xie, S.-P. (2008). On the origin of equatorial Atlantic biases in coupled general circulation models. *Climate Dynamics*, *31*(5), 587–598. https://doi.org/10.1007/s00382-008-0364-z

Rowell, D. P., Folland, C. K., Maskell, K., Owen, J. A., & Ward, M. N. (1992). Modelling the influence of global sea surface temperatures on the variability and predictability of seasonal Sahel rainfall. *Geophysical Research Letters*, *19*(9), 905–908. https://doi.org/doi:10.1029/92GL00939

Sanogo, S., Fink, A. H., Omotosho, J. A., Ba, A., Redl, R., & Ermert, V. (2015). Spatio-temporal characteristics of the recent rainfall recovery in West Africa. *International Journal of Climatology*, *35*(15), 4589–4605. https://doi.org/10.1002/joc.4309

Scannell, C., Booth, B. B. B., Dunstone, N. J., Rowell, D. P., Bernie, D. J., Kasoar, M., et al. (2019). The Influence of Remote Aerosol Forcing from Industrialized Economies on the Future Evolution of East and West African Rainfall. *Journal of Climate*, *32*(23), 8335–8354. https://doi.org/10.1175/JCLI-D-18-0716.1

Schneider, T., Bischoff, T., & Haug, G. H. (2014a). Migrations and dynamics of the intertropical convergence zone. *Nature*, *513*, 45. Retrieved from https://doi.org/10.1038/nature13636

Schneider, U., Becker, A., Finger, P., Meyer-Christoffer, A., Ziese, M., & Rudolf, B. (2014b). GPCC's new land surface precipitation climatology based on quality-controlled in situ data and its role in quantifying the global water cycle. *Theoretical and Applied Climatology*, *115*(1–2), 15–40. https://doi.org/10.1007/s00704-013-0860-x

Schubert, W. H., Ciesielski, P. E., Stevens, D. E., & Kuo, H.-C. (1991). Potential vorticity modeling of the ITCZ and the Hadley circulation. *Journal of the Atmospheric Sciences*, *48*(12), 1493–1509.

Shekhar, R., & Boos, W. R. (2017). Weakening and Shifting of the Saharan Shallow Meridional Circulation during Wet Years of the West African Monsoon. *Journal of Climate*, *30*(18), 7399–7422. https://doi.org/10.1175/JCLI-D-16-0696.1

Shi, X., Chen, X., Dai, Y., & Hu, G. (2020). Climate Sensitivity and Feedbacks of BCC-CSM to Idealized CO2 Forcing from CMIP5 to CMIP6. *Journal of Meteorological Research*, *34*(4), 865–878. https://doi.org/10.1007/s13351-020-9204-9

Shonk, J. K. P., Turner, A. G., Chevuturi, A., Wilcox, L. J., Dittus, A. J., & Hawkins, E. (2020). Uncertainty in aerosol radiative forcing impacts the simulated global monsoon in the 20th century. *Atmospheric Chemistry and Physics*, *20*(23), 14903–14915. https://doi.org/10.5194/acp-20-14903-2020

Sillmann, J., Kharin, V. V, Zhang, X., Zwiers, F. W., & Bronaugh, D. (2013). Climate extremes indices in the CMIP5 multimodel ensemble: Part 1. Model evaluation in the present climate. *Journal of Geophysical Research: Atmospheres*, *118*(4), 1716–1733. https://doi.org/doi:10.1002/jgrd.50203

Skinner, C. B., Ashfaq, M., & Diffenbaugh, N. S. (2012). Influence of Twenty-First-Century Atmospheric and Sea Surface Temperature Forcing on West African Climate. *Journal of Climate*, *25*(2), 527–542. https://doi.org/10.1175/2011JCLI4183.1

Song, F., Leung, L. R., Lu, J., Dong, L., Zhou, W., Harrop, B., & Qian, Y. (2021). Emergence of seasonal delay of tropical rainfall during 1979–2019. *Nature Climate Change*. https://doi.org/10.1038/s41558-021-01066-x

Stige, L. C., Stave, J., Chan, K.-S., Ciannelli, L., Pettorelli, N., Glantz, M., et al. (2006). The effect of climate variation on agro-pastoral production in Africa. *Proceedings of the National Academy of Sciences of the United States of America*, *103*(9), 3049 LP – 3053. https://doi.org/10.1073/pnas.0600057103

Sultan, B., & Gaetani, M. (2016). Agriculture in West Africa in the Twenty-First Century: Climate Change and Impacts Scenarios, and Potential for Adaptation. *Frontiers in Plant Science*, *7*,

1262. https://doi.org/10.3389/fpls.2016.01262

Swart, N. C., Cole, J. N. S., Kharin, V. V, Lazare, M., Scinocca, J. F., Gillett, N. P., et al. (2019). The Canadian Earth System Model version 5 (CanESM5.0.3). *Geoscientific Model Development*, *12*(11), 4823–4873. https://doi.org/10.5194/gmd-12-4823-2019

Tatebe, H., Ogura, T., Nitta, T., Komuro, Y., Ogochi, K., Takemura, T., et al. (2019). Description and basic evaluation of simulated mean state, internal variability, and climate sensitivity in MIROC6. *Geoscientific Model Development*, *12*(7), 2727–2765. https://doi.org/10.5194/gmd-12-2727-2019

Taylor, C. M., Belušić, D., Guichard, F., Parker, D. J., Vischel, T., Bock, O., et al. (2017). Frequency of extreme Sahelian storms tripled since 1982 in satellite observations. *Nature*, *544*(7651), 475–478. https://doi.org/10.1038/nature22069

Taylor, K. E., Stouffer, R. J., & Meehl, G. A. (2012). An overview of CMIP5 and the experiment design. *Bulletin of the American Meteorological Society*. https://doi.org/10.1175/BAMS-D-11-00094.1

Thorncroft, C. D., & Blackburn, M. (1999). Maintenance of the African easterly jet. *Quarterly Journal of the Royal Meteorological Society*, *125*(555), 763–786. https://doi.org/10.1002/qj.49712555502

Trenberth, K. E., & Caron, J. M. (2001). Estimates of meridional atmosphere and ocean heat transports. *Journal of Climate*, *14*(16), 3433–3443.

Vellinga, M., Roberts, M., Vidale, P. L., Mizielinski, M. S., Demory, M.-E., Schiemann, R., et al. (2016). Sahel decadal rainfall variability and the role of model horizontal resolution. *Geophysical Research Letters*, *43*(1), 326–333. https://doi.org/10.1002/2015GL066690

Villamayor, J., & Mohino, E. (2015). Robust Sahel drought due to the Interdecadal Pacific Oscillation in CMIP5 simulations. *Geophysical Research Letters*, *42*(4), 1214–1222. https://doi.org/doi:10.1002/2014GL062473

Voldoire, A., Saint-Martin, D., Sénési, S., Decharme, B., Alias, A., Chevallier, M., et al. (2019). Evaluation of CMIP6 DECK Experiments With CNRM-CM6-1. *Journal of Advances in Modeling Earth Systems*, *11*(7), 2177–2213. https://doi.org/10.1029/2019MS001683

Whittleston, D., Nicholson, S. E., Schlosser, A., & Entekhabi, D. (2017). Climate Models Lack Jet–Rainfall Coupling over West Africa. *Journal of Climate*, *30*(12), 4625–4632. https://doi.org/10.1175/JCLI-D-16-0579.1

Wilcox, L. J., Highwood, E. J., Booth, B. B. B., & Carslaw, K. S. (2015). Quantifying sources of inter-model diversity in the cloud albedo effect. *Geophysical Research Letters*, *42*(5), 1568–1575. https://doi.org/doi:10.1002/2015GL063301

Williams, K. D., Copsey, D., Blockley, E. W., Bodas-Salcedo, A., Calvert, D., Comer, R., et al. (2018). The Met Office Global Coupled Model 3.0 and 3.1 (GC3.0 and GC3.1) Configurations. *Journal of Advances in Modeling Earth Systems*, *10*(2), 357–380. https://doi.org/doi:10.1002/2017MS001115

Willmott, C. J., Matsuura, K., & Legates, D. R. (2001). Terrestrial air temperature and precipitation: monthly and annual time series (1950–1999). *Center for Climate Research Version*, *1*.

Wu, M.-L. C., Reale, O., Schubert, S. D., Suarez, M. J., & Thorncroft, C. D. (2012). African Easterly Jet: Barotropic Instability, Waves, and Cyclogenesis. *Journal of Climate*, *25*(5), 1489–1510. https://doi.org/10.1175/2011JCLI4241.1

Yukimoto, S., Kawai, H., Koshiro, T., Oshima, N., Yoshida, K., Urakawa, S., et al. (2019). The Meteorological Research Institute Earth System Model Version 2.0, MRI-ESM2.0: Description

and Basic Evaluation of the Physical Component. *Journal of the Meteorological Society of Japan. Ser. II*, *97*(5), 931–965. https://doi.org/10.2151/jmsj.2019-051

Zhang, S., Stier, P., Dagan, G., & Wang, M. (2022). Anthropogenic Aerosols Modulated 20th-Century Sahel Rainfall Variability Via Their Impacts on North Atlantic Sea Surface Temperature. *Geophysical Research Letters*, *49*(1), e2021GL095629. https://doi.org/https://doi.org/10.1029/2021GL095629

Ziehn, T., Chamberlain, M. A., Law, R. M., Lenton, A., Bodman, R. W., Dix, M., et al. (2020). The Australian Earth System Model: ACCESS-ESM1.5. *Journal of Southern Hemisphere Earth Systems Science*. Retrieved from https://doi.org/10.1071/ES19035

993 Figures

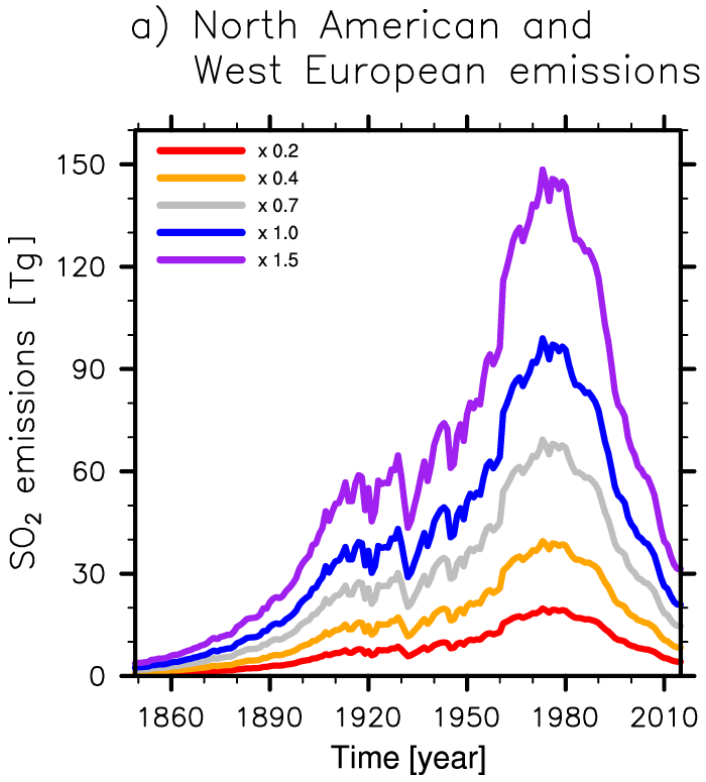

994

995 **Figure 1**: North American [170°W-40°W; 20°-70°N] and West European [20°W-50°E; 35°-
996 70°N] anthropogenic SO_2 emissions that were used for each scaling [in Tg].

997

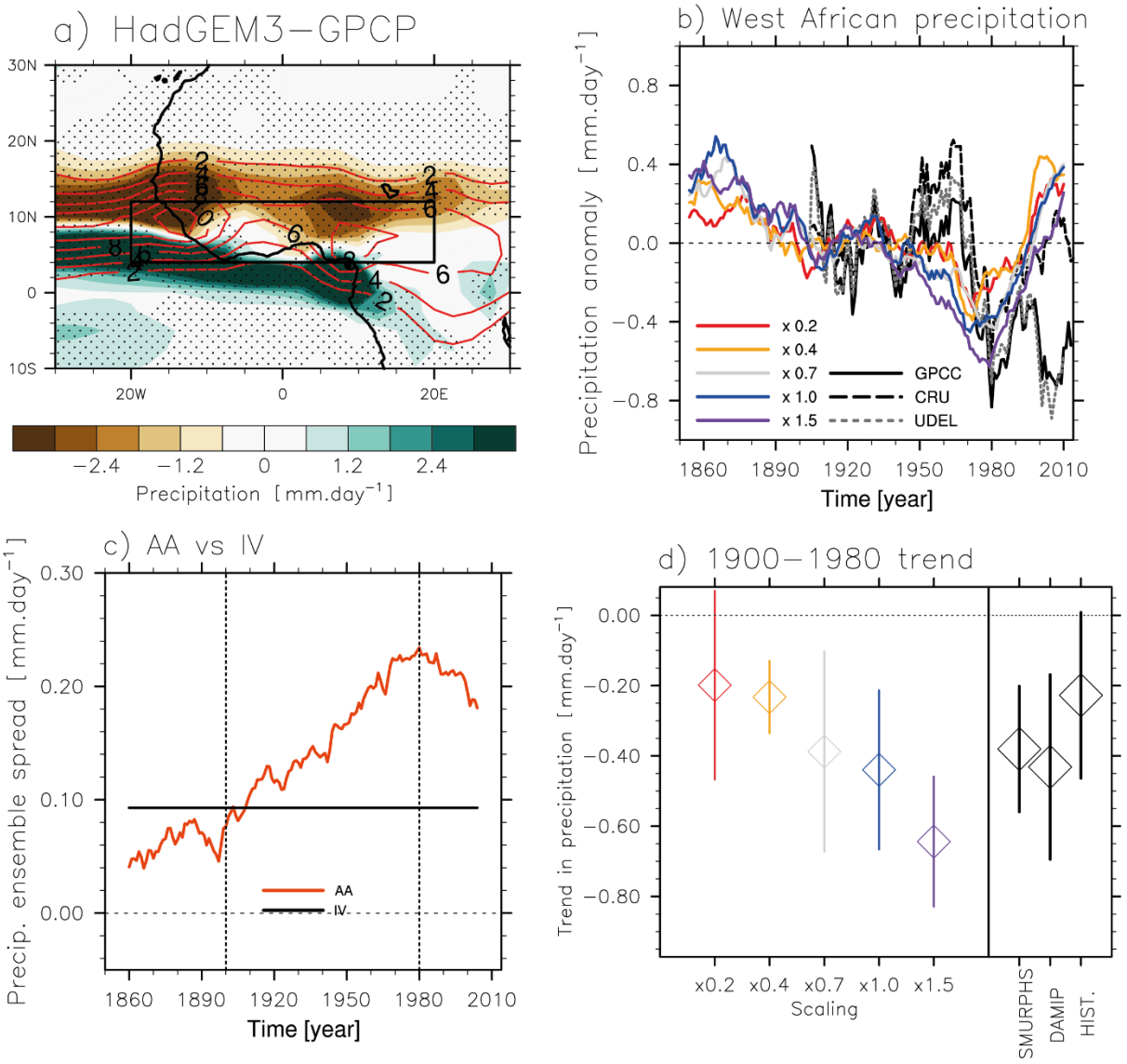

Figure 2: a) Contours show the observed precipitation (GPCP; mm.day^{-1}), averaged over July-September 1979—2014. Colours show the bias of HadGEM3-GC31, relative to GPCP. Stippling indicates where the bias is significantly different to zero according to a Student's *t* test at the 90% confidence level. The black box indicates the area that is used to compute the West African precipitation timeseries. b) Time series of West African precipitation anomalies [4°N-12°N; 20°W-20°E; mm.day^{-1}] for each scaling (colours) and GPCC, CRU and UDEL (black and grey). Anomalies are computed relative to 1901-1930. c) Spread due to AA, defined as the standard deviation across the five ensemble means of the different scaling experiments (red) and internal variability (black), defined as the standard deviation across the different initial-condition members within a single scaling experiment. The resulting five standard deviations for each scaling experiment are subsequently averaged to represent an estimate of internal variability. The high-frequency variability is first removed with a 21-year running mean. d) Linear trends in West African precipitation between 1900 and 1980 [mm.day^{-1} over the 81 years] for each scaling, for the SMURPHS ensemble, the CMIP6 DAMIP aerosol only and historical ensembles. Diamonds show the ensemble-mean and the vertical lines the standard deviation computed from the ensemble-mean of each scaling and each CMIP6 three-member ensemble.

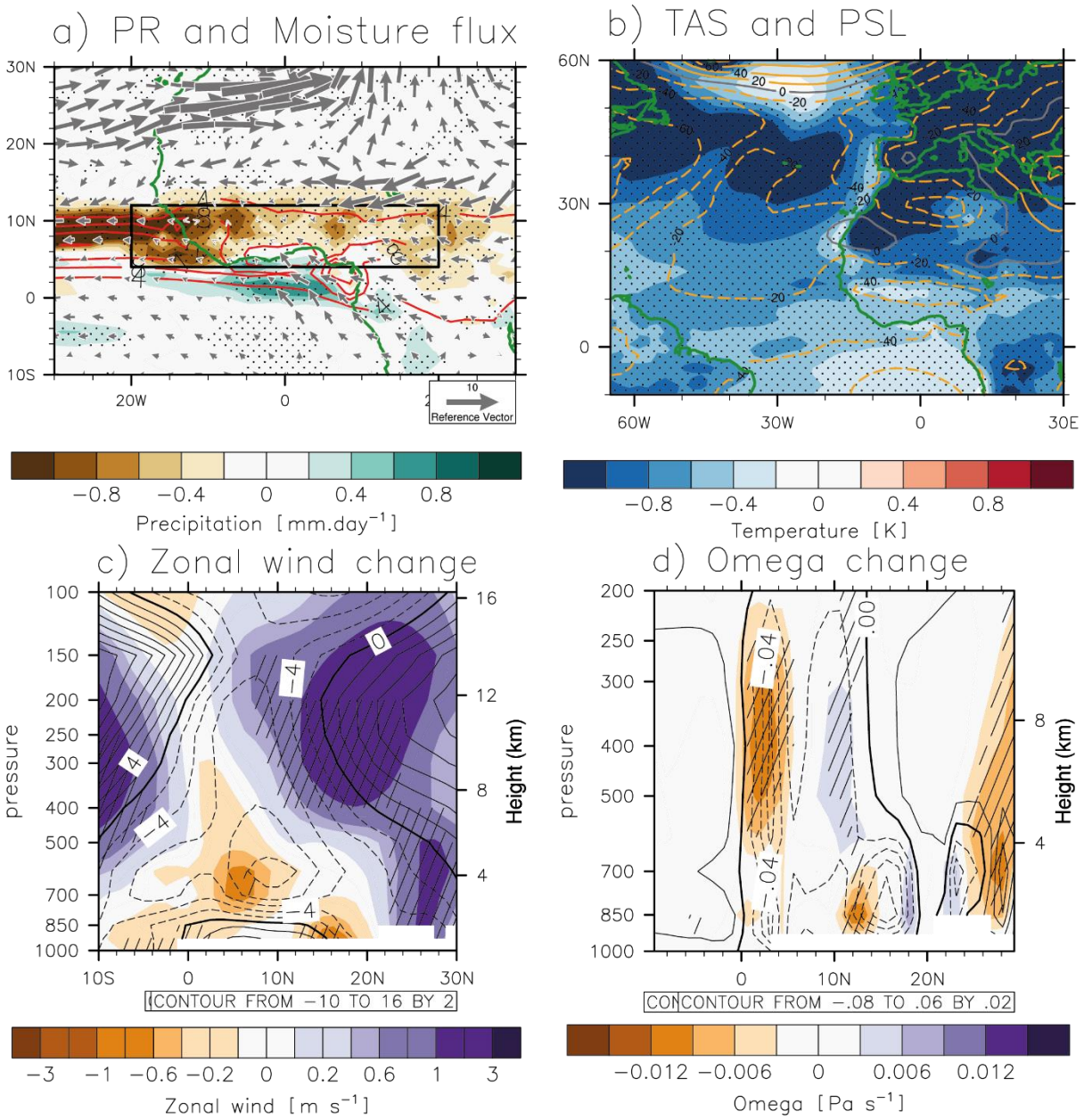

Figure 3: Full uncertainty in effects of anthropogenic aerosols is shown by showing differences in 1900-1980 trend between the x1.5 and x0.2 scalings. a) Effects on precipitation [colours, mm.day^{-1}] and moisture flux [vectors; g.kg^{-1} m.s^{-1}]. Red contours indicate the 1900-1980 mean climatology of the x0.2 scaling. The black box indicates the area that is used to compute the West African precipitation timeseries. b) Effects on surface air temperature [colours; K] and sea-level pressure [negative/positive values are displayed with dashed/solid contours; Pa]. c) Effects on zonal wind, averaged from 10°W to 10°E and given between 10°S and 30°N, obtained by the difference between the x1.5 and x0.2 scalings [colours; m.s^{-1}]. Climatology is defined as the average of the zonal wind of the scaling x0.2 from 1900 to 1980 [contours; m.s-1]. d) As in (c) but for omega [Pa.s^{-1}] (negative values in omega indicate ascent). Stippling (a-b) and hatchings (c-d) indicate that differences are significantly different to zero, according to a Monte Carlo approach and at the 95% confidence level.

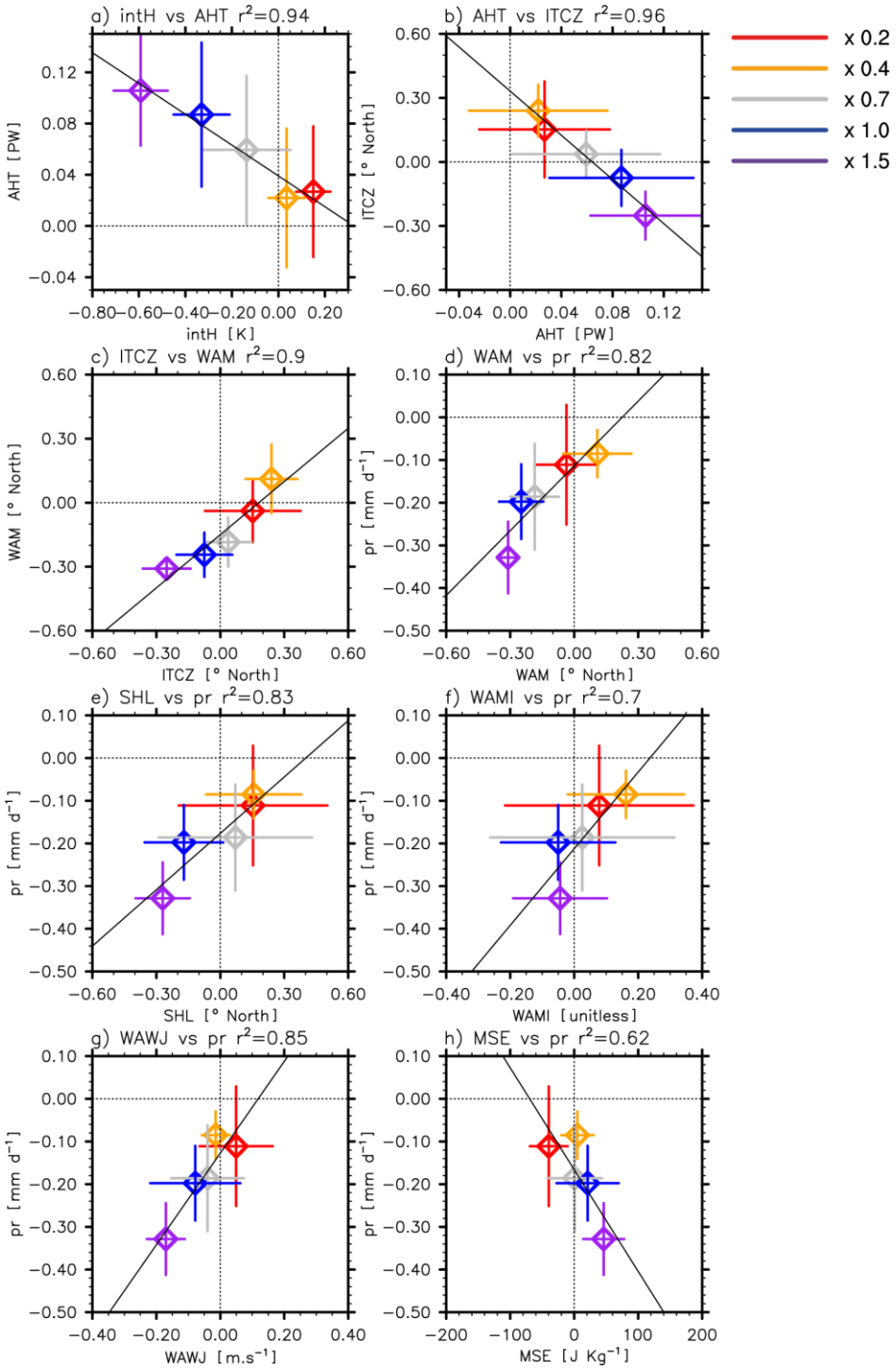

Figure 4: Scatter plots of the 1900-1980 trends in a) global inter-hemispheric temperature contrast and cross-equatorial atmospheric heat transport, b) global cross-equatorial heat transport and meridional location of the global intertropical convergence zone (i.e. global zonal mean in precipitation), c) meridional location of the global intertropical convergence zone and meridional location of the West African Monsoon, and West African precipitation in function of the d) meridional location of the West African Monsoon, e) meridional location of the Saharan Heat low, f) WAMI index, g) strength of the west African westerly jet and h) meridional gradient in moist static energy. Vertical and horizontal lines indicate the

uncertainty, defined as two times the standard error. Each scaling is shown with a colour (see Figure 1b). Metrics are described in Sect. 3.2.

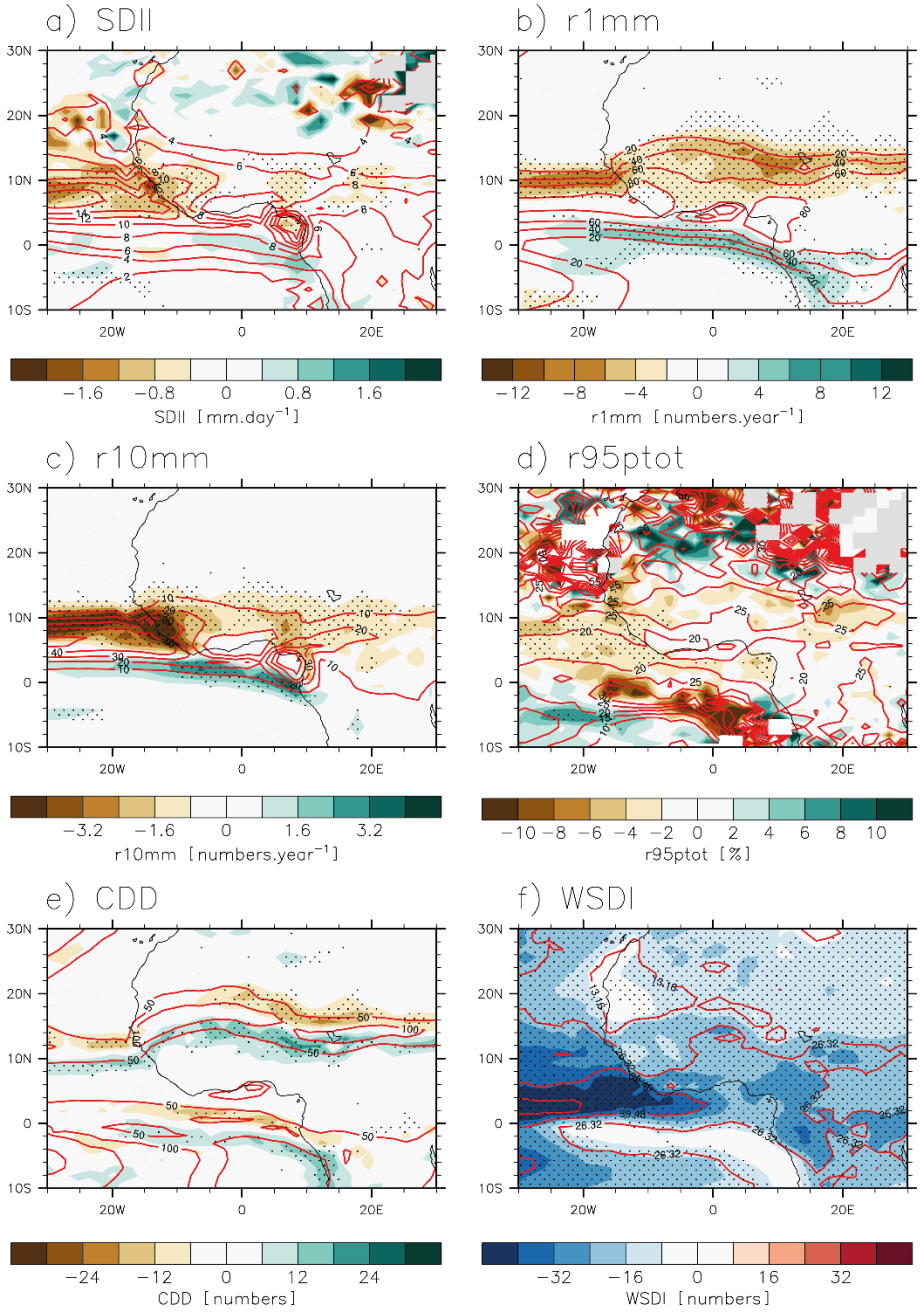

Figure 5. Full uncertainty in effects of anthropogenic aerosols is shown by showing differences between the scaling x1.5 and scaling x0.2, averaged over the period 1950-1980 and in JAS. a) Effects on SDII [in mm.day^{-1}], b) R1mm [in days], c) R10mm [in days], d) R95ptot [in %], e) CDD [in numbers of dry spells] and f) WSDI [in numbers of warm spells]. Red contours are the 1950-1980 climatology, taken from the scaling x0.2. Stippling indicate that anomalies are significant according to a Student's *t* test and at the 95% confidence level. See metrics in Sect. 3.2.8.

Experiment	x 0.2	x 0.4	x 0.7	x 1.0	x 1.5
x 0.2	0				
x 0.4	-0.034	0			
x 0.7	-0.189	-0.155	0		
x 1.0	**-0.241***	**-0.207***	-0.052	0	
x 1.5	**-0.445***	**-0.411***	**-0.256***	**-0.204***	0

Table 1: Difference in 1900—1980 West African precipitation trends [mm.day^{-1}], in summer (JAS) and between the ensemble-means. One star and bold values indicates that differences are significant at the 95% confidence interval, following a Monte-Carlo approach and with two-sided test. Precipitation is averaged between 4°-12°N and 20°W-20°E.

Models	Institutions	References
ACCESS-ESM1-5	Australian Community Climate and Earth System Model, Australia	(Ziehn et al., 2020)
BCC-CSM2-MR	Beijing Climate Centre, China	(Shi et al., 2020)
CanESM5	Canadian Centre for Climate Modelling and Analysis, Canada	(Swart et al., 2019)
CNRM-CM6-1	Centre National de Recherches Météorologiques, France	(Voldoire et al., 2019)
FGOALS-G3	Chinese Academy of Sciences, China	(Li et al., 2020)
HADGEM3-GC31-LL	Met Office Hadley Centre, United Kingdom	(Kuhlbrodt et al., 2018)
GISS-E2-1-G	Goddard Institute for Space Studies, United States	(Kelley et al., 2020)
IPSL-CM6A-LR	Institut Pierre Simon Laplace, France	(Boucher et al., 2020)
MIROC6	Japanese modelling community, Japan	(Tatebe et al., 2019)
MRI-ESM2-0	Meteorological Research Institute, Japan	(Yukimoto et al., 2019)

1061 **Table 2**: List of DAMIP CMIP6 climate models used in the study

1062